Article

Correlating Experimental with Theoretical Studies for a New Ionic Liquid for Inhibiting Corrosion of Carbon Steel during Oil Well Acidification

Arafat Toghan [1,2,*], **Ahmed Fawzy** [3,4], **Abbas I. Alakhras** [1], **Moustafa M. S. Sanad** [5,*], **M. Khairy** [1,6] and **Ahmed A. Farag** [7,*]

[1] Chemistry Department, College of Science, Imam Mohammad Ibn Saud Islamic University (IMSIU), Riyadh 11623, Saudi Arabia
[2] Chemistry Department, Faculty of Science, South Valley University, Qena 83523, Egypt
[3] Department of Chemistry, Faculty of Applied Science, Umm Al-Qura University, Makkah 21955, Saudi Arabia
[4] Chemistry Department, Faculty of Science, Assiut University, Assiut 71516, Egypt
[5] Central Metallurgical Research & Development Institute, P.O. Box 87 Helwan 11421, Cairo, Egypt
[6] Chemistry Department, Faculty of Science, Benha University, Benha 13511, Egypt
[7] Egyptian Petroleum Research Institute (EPRI), Cairo 11727, Egypt
* Correspondence: arafat.toghan@yahoo.com or aatahmed@imamu.edu.sa (A.T.); mustafa_sanad2002@yahoo.com (M.M.S.S.); ahmedafm@yahoo.com (A.A.F.)

Abstract: During the mandatory acidification process in the oil and gas industry, carbon steel unfortunately suffers significant corrosion damage. From this perspective, for the first time a new ionic liquid called 1-(2-(4-bromophenyl)-2-oxoethyl)-4-(tert-butyl)pyridin-1-ium bromide (ILB) has been used as an effective inhibitor for the carbon steel corrosion in aggressive HCl solution (15%) at 298 K. The experiments were managed with a number of different chemical and electrochemical techniques including weight loss, potentiodynamic polarization (PDP), and impedance spectroscopy (EIS). ILB has good inhibitory performance as an acidizing corrosion inhibitor for carbon steel even at low dosing levels of 1×10^{-3} M. The findings were promising as an inhibition efficiency of about 97% was achieved when ILB was added at low concentrations to the corrosive media. EIS results showed a significant rise in charge transfer resistance (R_{ct}) values with increasing doses of ILB. PDP studies confirmed that ILB is a mixed type and obey Langmuir adsorption isotherm with chemical nature. The metal surface morphologies were inspected using a Scanning Electron Microscope (SEM) and an Atomic Force Microscope (AFM). Additionally, Density Functional Theory (DFT) and Molecular Dynamic Simulation (MDS) indicates that ILB molecules function as inhibitors more successfully. There is a high degree of concordance between practical and theoretical studies.

Keywords: carbon steel; oil well acidization; acid corrosion; ionic liquid inhibitor; DFT; surface morphology; SEM; AFM; EIS

1. Introduction

The oil and gas sector are growing as a result of increased oil and gas extraction, which makes it necessary to rebuild both new and old oil wells [1–4]. In petroleum wells, chloride salts can be found dissolved in formation water or dispersed in crude oil. Formation water is subsurface water created as a byproduct of crude oil production. Most oil and gas fields often inject producing wells with high concentrations of acid solutions (40–60% vol), a procedure known as acidizing. This acidifying process dissolves rocky soil, minerals, and foreign material in the well's soil, producing channels and enhancing oil and gas productivity. Acid inclusion raises reservoir permeability by eroding mineral rocks [5]. On the other hand, integrated acid results in severe monetary loss and tubular

steel corrosion [6–8]. The corrosion inhibitors are certain molecules composed of lone pairs of electrons, a high electron cloud of aromatic rings, double and triple bond conjugations, and additional adsorption centers [9]. These adsorption centers generate both an adsorbed layer and a metal orbital coordinating bond [10]. According to a literature review, the oil and gas industry frequently seeks corrosion inhibitors such as Schiff base, quaternary ammonium salts, and other inhibitors [11,12]. However, educating about the importance of protecting the environment from long-present dangerous inhibitors is only partially effective [13,14]. A further study was conducted in order to create non-toxic, environmentally friendly corrosion inhibitors, such as surfactant, biological extract, ionic liquid, and others [15–22]. Ionic liquids (ILs) have attracted the attention of scientists in recent years as potential corrosion inhibitors for specific metals and alloys. Ionic liquids are usually salts of organic anions (such as pyrrolidinium, imidazolium, or pyridinium) and inorganic cations (such as chloride, bromide, or iodide). Ionic liquids' remarkable qualities as long-lasting, environmentally benign chemicals with the ability to dissolve a variety of inorganic and organic components are the reason for their expanding application. Ionic solutions based on imidazolium have become popular in recent years as corrosion inhibitors in acidic settings. ILs are utilized widely due to their non-toxicity, low m.p., and liquid condition at ambient temperature [23]. Due to their capacities to form micelles and lower interfacial tension of aqueous wetting, which enables simple adsorption of corrosion-inhibitors molecules, ILs have recently emerged as a significant grade of corrosion mitigation [24,25]. Furthermore, intermolecular synergy and inhibitor adhesion on the metal surface are made possible by cation and anionic groups [26]. However, acidification is the most efficient way to increase production and explore for oil, but it is very corrosive to the metal. Therefore, in the current study we present for the first time a novel, potent and non-toxic corrosion inhibitor of ionic liquid based pyridinium (ILB) in a very strong acidic environment (15% HCl), i.e., in real conditions. The choice of ILB in particular is based on many advantages, the most important of which is that it is an environmentally friendly corrosion inhibitor, and its chemical composition is unique. In addition, it is effective in lowering acidic media concentrations. The results of this work confirm the high efficiency of this type of material in resisting corrosion of steel, which may open the way for real practical application.

2. Experimental

2.1. Materials

The composition of the carbon steel specimens used in this research is as follows: 10.73% Cr, 7% Ni, 7% Si, 4.55% Al, and the rest is Fe. The carbon steel dimensions for the weight loss measurements were 7.0 cm × 2.0 cm × 0.2 cm. To get the electrochemical data, a carbon steel electrode with a surface area of 1 cm^2 was used. Prior to the trial, the steel samples were absorbed, polished, washed with distilled water, and then treated with a 1:1 combination of ethanol and acetone. The 15% HCl aggressive solution was produced using analytical grade HCl. The ionic liquid 1-(2-(4-bromophenyl)-2-oxoethyl)-4-(tert-butyl)pyridin-1-ium bromide (ILB) that was the subject of the investigation was supplied from Sigma-Aldrich company. Figure 1 shows the molecular structure of ILB.
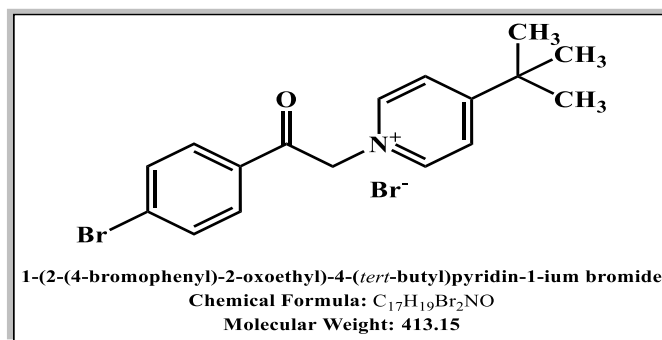
1-(2-(4-bromophenyl)-2-oxoethyl)-4-(*tert*-butyl)pyridin-1-ium bromide
Chemical Formula: $C_{17}H_{19}Br_2NO$
Molecular Weight: 413.15

Figure 1. Chemical structure of ILB.

2.2. Weight Loss Measurements

The ASTM standard is applied when conducting tests on weight loss [27]. In each weight loss experiment, steel coupon specimens with dimensions of 7 cm × 2 cm × 0.3 cm were used. After immersion duration (8 h), the weight loss of steel in aggressive solution (measured in mg cm²) with and without the presence of various concentrations of ILB inhibitor was determined. The samples' surfaces were cleaned by repeatedly washing the corrosion product in bi-distilled water, followed by drying. The following equations were used to determine the corrosion rate (*CR*), surface coverage (*θ*), and inhibition efficiency (*IE*$_{WL}$ %) [28]:

$$CR = \frac{\Delta W}{St} \tag{1}$$

$$\theta = \frac{CR - CR_{inh}}{CR} \tag{2}$$

$$IE_{WL} \, (\%) = \theta \times 100 \tag{3}$$

where, *CR* and *CR*$_{inh}$ are the rates of steel corrosion in the aggressive solution in the absence and presence of various ILB concentrations, respectively. *ΔW*, *S*, and *t* signify the weight loss (mg), carbon steel surface area (cm²), and immersion time (h), respectively.

2.3. Electrochemical Investigation

An Origalys potentiostat supported with Origa Master was used to conduct and calculate the electrochemical outcomes. The employed three-electrode cell arrangement used carbon steel as the working electrode, calomel as the reference electrode, and Pt-wire as the counter electrode. The steel electrode was left in the aggressive solution for 30 min. to get an equilibrium potential. The EIS tests used a range of frequencies, from 10^5 to 10^{-2} Hz with 10 mV of potential. Similar to this, potentiodynamic polarization tests were determined by measuring the steel substrate at a rate of 0.1 mVs^{-1} between a potential range of ±250 mV.

2.4. Theoretical Calculations

Recent developments in the study of organic molecule-mediated corrosion inhibition processes have shown the utility of quantum chemical calculations. On the probability of electron transfer between the molecules that are adsorbed and the Fe surface, they provide helpful relationships. It is the relationship between the effectiveness of the molecular shapes under investigation. When analyzing the connection between inhibition effectiveness and electronic structure, DFT analysis is used because it is simple, quick, and accurate. This part of the work examines the molecular and electronic structures of the ILB molecule to show the relationship between the molecular structure of this compound and

its inhibitory effectiveness. As theoretical parameters, it was possible to determine the energies of the lowest unoccupied and highest occupied molecular orbitals (E_{LUMO} & E_{HOMO}), the energy gap ($\Delta E = E_{LUMO} - E_{HOMO}$), hardness ($\eta$), electronegativity ($\chi$), softness ($\sigma$), and the fraction of transferred electrons (ΔN). These descriptors are included with the accompanying equations [29].

$$I = -E_{HOMO} \tag{4}$$

$$A = -E_{LUMO} \tag{5}$$

$$\chi = \frac{I + A}{2} \tag{6}$$

$$\eta = \frac{I - A}{2} \tag{7}$$

$$\sigma = \frac{1}{\eta} \tag{8}$$

$$\Delta N = \frac{(\chi_{Fe} - \chi_{Inh})}{2(\eta_{Fe} - \eta_{Inh})} \tag{9}$$

The DFT/B3LYP method, the 6-311G*(d,p) basis set, and the Gaussian 09 software package were used to calculate the ILB molecule calculations. The adsorption behavior of the ILB inhibitor molecule on the Fe(110) surface was examined using molecular dynamic (MD) models. Using the programme Material Studio 2020, MD simulations were carried out.

2.5. Surface Analysis

The surface image of the film created on carbon steel in the absence and presence of an optimum concentration of ILB inhibitor in the aggressive solution for an 8-h immersion time was captured and studied using SEM equipment. For the 3-D image, AFM micrographic analysis was used to quantify the surface roughness of metal after it was immersed in an aggressive electrolyte in the presence and absence of ionic liquid for approximately 8 h.

3. Result and Discussion

3.1. Electrochemical Impedance Spectroscopy (EIS)

Figure 2a–c depicts the Nyquist plots along with the associated Bode plots, and the equivalent chemical circuit of carbon steel in the aggressive solution without and with ILB, respectively. The width of the capacitive loop of the Nyquist plots widens as the ILB concentration increases, as shown in Figure 2a. As a result, as the ILB concentration increases, so does the charge transfer resistance (R_{ct}), increasing the effectiveness of the inhibition [30]. This is because any active reaction sites on the steel surface are covered by ILB molecules, preventing them from coming into contact with the strong solution. On the Nyquist graphs, the typical charge transfer-controlled corrosion reaction process is depicted as a single depressed capacitive semicircle with the center under the real line. As shown in Figure 2b, increasing ILB concentration results in a wide and broad shift in the Bode modulus impedance, indicating a delay in the corrosion process. As shown in Figure 2c, the circuit model R_s (QR_{ct}) was fitted to the gathered data set with (R_s) which stands for solution resistance, (R_{ct}) for charge transfer resistance, and (Q) for constant phase element (CPE). The non-perfect semi-circle nature of Nyquist plots is caused by a rough fractal surface, which is associated with the formation of an absorbed inhibitor layer as well as corrosion products [31]. As a result, the capacitance provided by the constant phase element (CPE) is denoted by the following relationship [32]:

$$Z_{CPE} = \frac{1}{Y_o(j\omega)^n} \tag{10}$$

Z_{CPE} stands for CPE impedance, while Y_o, n, and j represent the scale and proponent of CPE, accordingly ($\sqrt{-1}$). Similar to that, f (Hz) is the frequency, and $\omega = 2\pi f$.
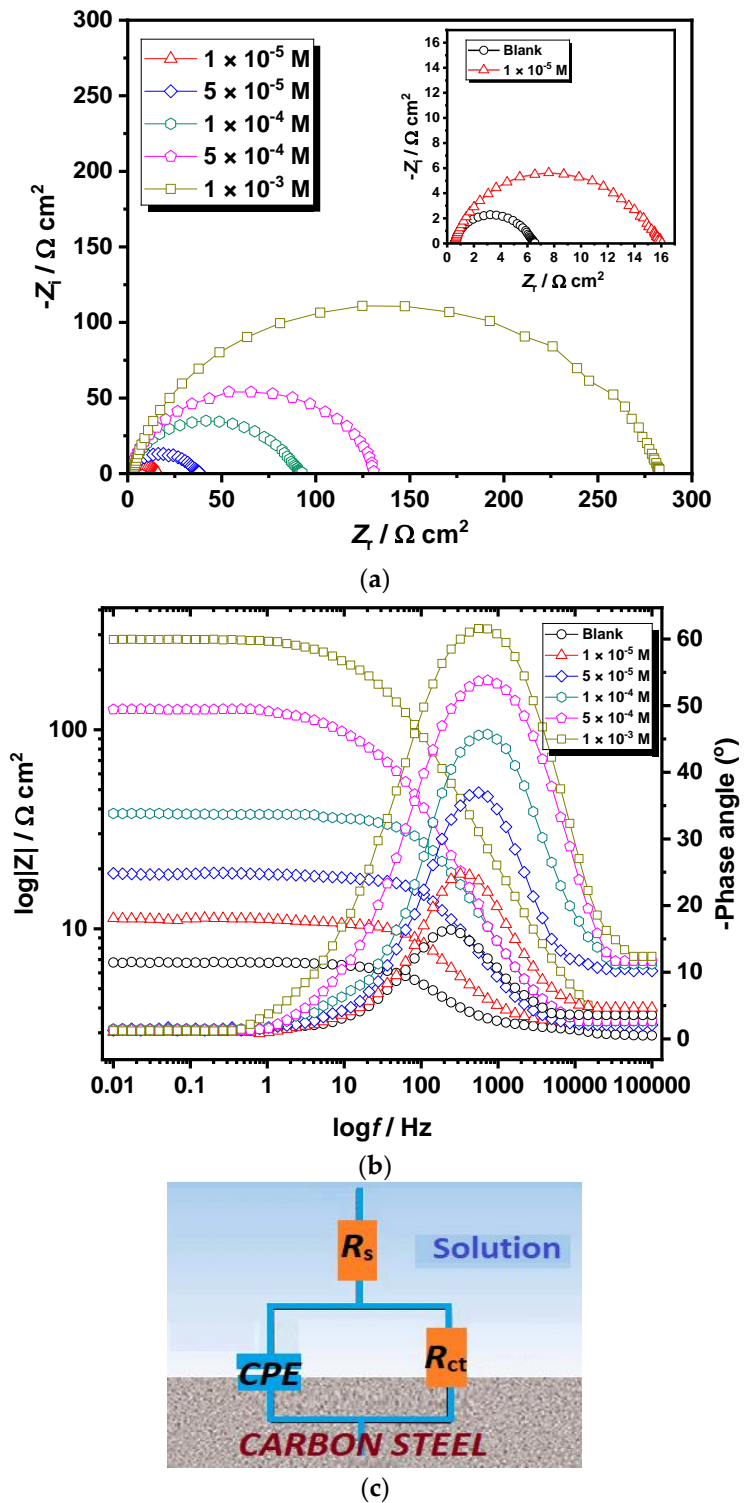

(**a**)

(**b**)

(**c**)

Figure 2. EIS curves for carbon steel in the aggressive solution in the absence and presence of various concentrations of ILB at 298 K: (**a**) Nyquist, (**b**) Bode, and (**c**) equivalent chemical circuit.

Table 1 displays the data obtained from EIS experiments at 298 K. In order to determine the inhibitory efficiency (IE_{EIS}, %) derived from the impedance measurements, the following expression was used [33]:

$$\eta_{EIS} = \frac{R_{ct(inh.)} - R_{ct}}{R_{ct(inh.)}} \times 100 \tag{11}$$

where, R_{ct} and $R_{ct(inh.)}$ are the charge transfer resistances of a carbon steel electrode in the aggressive acid solution without and with the examined inhibitor. Table 1 demonstrates that R_{ct} values were greatly increased as the ILB concentration was increased. It is possible that the protective layer deposition on the steel surface, which creates barriers for charge transports, is what causes the observed rise in R_{ct} values with rising ILB concentrations. Given that the estimates for the *n* parameter range from 0.79 to 0.89, it is most probable that the ILB adsorption process has reduced the heterogeneity of the steel surface [34].

Table 1. Electrochemical impedance parameters of carbon steel in the aggressive acid solution and in the presence of different concentration of ILB at 298 K.

ILB Conc. (M)	R_s (Ω cm²)	$Y_0 \times 10^{-4}$ (Ω^{-1}s^n cm^{-2})	*n*	R_{ct} (Ω cm²)	η_{EIS} (%)
0	0.8	1.85	0.79	6	–
1 × 10⁻⁵	1.3	6.47	0.82	14	57.1
5 × 10⁻⁵	1.8	5.66	0.86	36	83.3
1 × 10⁻⁴	2.0	3.72	0.87	89	93.3
5 × 10⁻⁴	1.9	4.65	0.88	131	95.4
1 × 10⁻³	2.1	5.32	0.89	280	97.9

3.2. Potentiodynamic Polarization Study

The potentiodynamic polarization (PDP) profiles of carbon steel in the aggressive solution, without and with varying concentrations of ILB, are shown in Figure 3. The resulting polarization curves were used to evaluate the values of corrosion potential (E_{corr}), corrosion current densities (i_{corr}), as well as cathodic and anodic Tafel slopes (β_c & β_a). The values of inhibition efficiencies (η_{PDP}) were calculated via the following equation [35]:

$$\eta_{PDP} = \frac{i_{corr} - i_{corr(inh.)}}{i_{corr}} \times 100 \tag{12}$$

i_{corr} and $i_{corr(inh.)}$ represent the current densities of steel corrosion without and with ILB, respectively. Table 2 summarizes these parameters at 298 K. The value of i_{corr} was set to decrease while η_{PDP} increased as ILB concentration increased. This demonstrated that the protective effect of ILB molecules on carbon steel became greater as the inhibitor concentration increased. At a concentration of 1 × 10⁻³ M ILB, the highest corrosion inhibition efficiency was 97.3%.
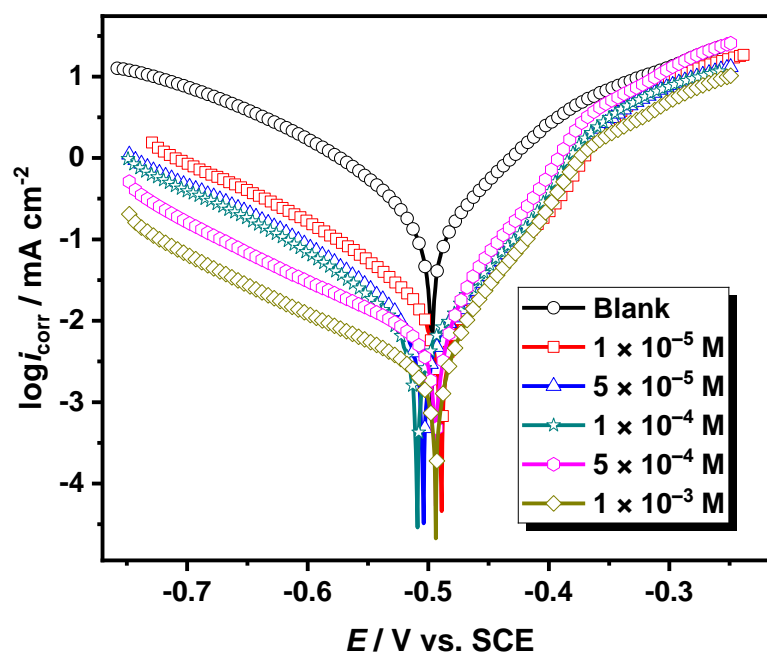
Figure 3. Potentiodynamic polarization curves of carbon steel in the aggressive solution in the absence and presence of various concentrations of ILB at 298 K.

As shown in Figure 3, the polarization curves of the cathode and anode were dissimilar in the presence of ILB rather than in the absence. These results showed that the examined inhibitor prevented not only metal dissolution but also hydrogen evolution. The polarization curves also revealed that cathode changes were more visible than anode changes. Furthermore, the corrosion potential (E_{corr}) shifted slightly when compared to the curve obtained in the absence of the inhibitor. ILB is thus classified as a mixed corrosion inhibitor [36]. Additionally, Table 2 shows that when the ILB was added, the values of both β_c and β_a scarcely changed, indicating that the hydrogen-evolution mechanism did not change. This could be as a result of the ILB molecule coating the carbon steel surface, which lowers the area of reactional active sites while remaining unaffected by the charge transfer process of hydrogen evolution.

Table 2. Potentiodynamic polarization parameters of carbon steel in the aggressive solution in the absence and presence of various concentrations of ILB at 298 K.

ILB Conc. (M)	$-E_{corr}$ (mV)	i_{corr} (mA.cm^{-2})	β_a (mV dec^{-1})	$-\beta_c$ (mV dec^{-1})	η_{PDP} (%)
0	0.494	3.662	112	135	–
1 × 10^{-5}	0.489	1.524	109	131	58.4
5 × 10^{-5}	0.499	0.641	108	126	82.5
1 × 10^{-4}	0.509	0.253	105	121	93.1
5 × 10^{-4}	0.496	0.176	101	118	95.2
1 × 10^{-3}	0.493	0.099	99	115	97.3

3.3. Weight-Loss Measurements

Table 3 shows the projected *CR* and η_{WL} values using the weight loss technique at various ILB concentrations at 298 K. Table 3 demonstrates that increasing ILB results in a decrease of the CR value. The weight loss data in Figure 4 is consistent with expectations because increasing the ILB dosage results in increased molecule adsorption on the carbon steel surface, reducing corrosion rate [37,38]. Furthermore, as ILB concentration rises, so does WL%, peaking at 93.5% at 1 × 10^{-3} M. This is caused by ILB adsorption on the surface

of carbon steel. ILB's ability to be inhibitive in the corrosive HCl solution reflects their powerful ability to form bonds with steel.

Table 3. Weight loss parameters of carbon steel in the aggressive solution in the absence and presence of various concentrations of ILB at 298 K.

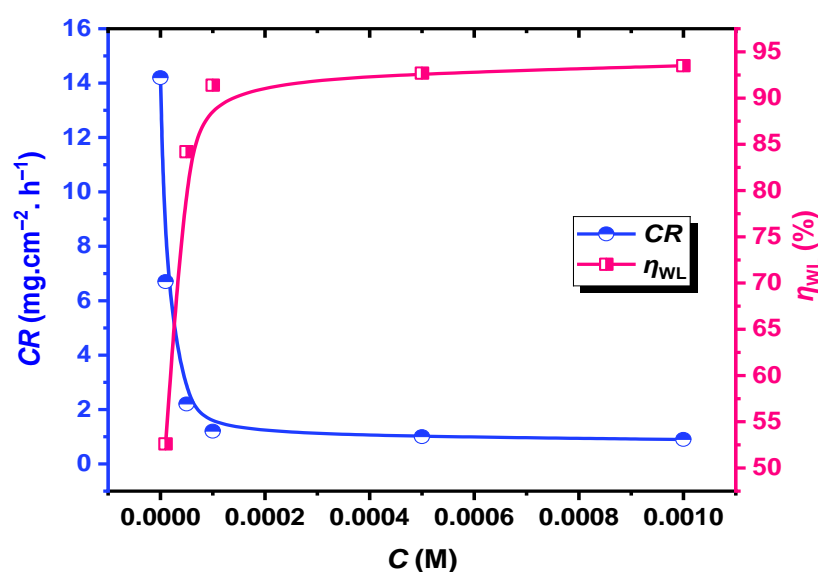| ILB Conc. (M)	CR (mg cm^{-2} h^{-1})	θ	η_{WL} (%)
0	14.2	–	–
1×10^{-5}	6.7	0.526	52.6
5×10^{-5}	2.2	0.842	84.2
1×10^{-4}	1.2	0.914	91.4
5×10^{-4}	1.0	0.927	92.7
1×10^{-3}	0.9	0.935	93.5

Figure 4. Plots of CR of carbon steel in the aggressive solution and η_{WL} (%) of ILB versus ILB concentration (C) at 298 K.

3.4. Adsorption Isotherms Study

Frumkin, Temkin, Freundlich, and Langmuir adsorption isotherms were used to investigate ILB adsorption on the carbon steel surface in the aggressive HCl solution. The weight loss results regarding the values of degree of surface coverage (θ) were used to determine which isotherm best described the adsorption process. The data were graphically tested by fitting to the adsorption isotherms listed above, as shown in Figure 5, and the correlation coefficient (R^2) was used to determine the best-fit isotherm. The Langmuir adsorption isotherm at 298 K fits the regression coefficient R^2 very well (Figure 5d), confirming the validity of the ILB adsorption on the carbon steel surface in the aggressive HCl solution. The following are the relationships of the studied adsorption isotherms' models [39]:

$$\text{Temkin: } K_{ads}C = e^{f\theta} \tag{13}$$

$$\text{Langmuir: } \frac{\theta}{(1-\theta)} = K_{ads}C \tag{14}$$

$$\text{Frumkin: } K_{ads}C = \left(\frac{\theta}{(1-\theta)}\right)e^{-2a\theta} \tag{15}$$
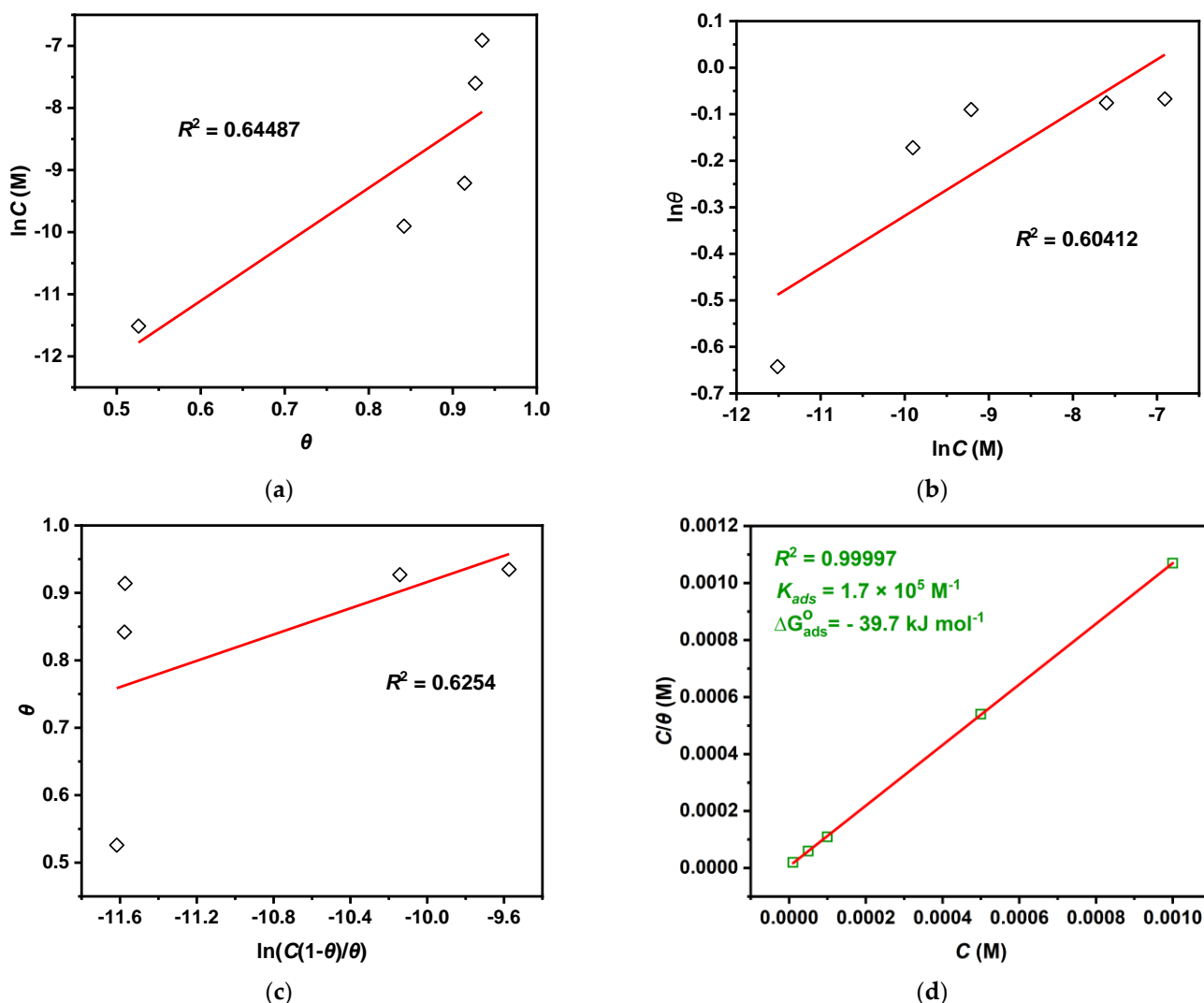
$$\text{Freundlich: } \theta = K_{ads}C^n \tag{16}$$

Figure 5. Adsorption isotherms' models: (**a**) Temkin, (**b**) Freundlich, (**c**) Frumkin, (**d**) Langmuir, for various ILB concentrations on the surface of carbon steel in the aggressive HCl solution at 298 K.

All adsorption sites are assumed to be equal and to have the same energetic potential as the Langmuir adsorption isotherm [15]. Adsorption parameters obtained from Langmuir isotherms are reported in Figure 5d. The intense adsorption of ILB on the steel surface in the corrosive HCl solution is confirmed by the high K_{ads} values. This is due to the presence of π-electrons and heteroatoms such as the quaternary N atom and O atom in ILB molecules. The standard free energy of adsorption (ΔG_{ads}^o) and K_{ads} were determined using the equations below [40]:

$$K_{ads} = \frac{1}{55.5} \exp\left(\frac{-\Delta G_{ads}^o}{RT}\right) \tag{17}$$

where R is the universal gas constant, T is the absolute temperature, and 55.5 is the water concentration given in M. A general rule of thumb is that values of ΔG_{ads}^o up to −20 kJ mol⁻¹ suggest physical adsorption, while values below −40 kJ mol⁻¹ indicate chemisorption [41]. Figure 5d shows that the studied ILB had a ΔG_{ads}^o value of −39.7 kJ mol⁻¹ (i.e., between −20 and −40 kJ mol⁻¹); indicating the adsorption behavior considered mixed between the physical and chemical adsorption.

3.5. Theoretical Studies

3.5.1. DFT Calculations

A quantum chemical calculation was performed to investigate the effect of electronic properties and molecular structure on the inhibition effectiveness of the ILB inhibitor and to confirm the experimental data obtained from gravimetric and electrochemical experiments [42]. Figure 6 depicts the optimized molecular structure provided by atomic numbering and the frontier molecular orbital density distributions (HOMO and LUMO) of ILB inhibitor provided by the B3LYP/6-31*G (d,p) method. The electron density of the HOMO is distributed at the tertiary butyl pyridinium fragment, while the LUMO is distributed at the other fragment of bromophenyl-oxoethyl, as shown in Figure 6. Table 4 displays the calculated quantum parameters of the ILB molecule. The E_{HOMO} values of ILB arehigh (−5.606 eV) while the E_{LUMO} value (−1.930 eV) is low, confirming the experimentally obtained inhibition efficiency. The presence of a higher electron density of an aromatic ring and lone pair of heteroatoms (O and N atoms) results in a high value of E_{HOMO} (−5.606 eV). The energy gap (ΔE_{GAP}) is a critical parameter that reveals an inhibitor molecule's activity [43]. The low ΔE_{GAP} value (3.676 eV) indicates higher reactivity and facilitates organic molecule adsorption on the steel surface, resulting in higher inhibition performance. The reduction of ΔE_{GAP} and E_{LUMO}, as well as the increase of E_{HOMO}, imply an increase in inhibitor efficiency [44]. Additionally, the softness (σ) is a crucial characteristic that can reveal the inhibitor compounds' capacity for adsorption. These can forecast the inhibitor compounds' strong affinity for adsorption, which is consistent with the findings of the experiments [45]. The ability of electrons to transfer from an inhibitor to a metal is measured by the value of ΔN. The value of ΔN, on the other hand, does not represent the actual number of electron transfers; rather, it represents a potential. Electrons are transported from the adsorbent molecules to the Fe atoms on the metallic surface if ΔN is positive. This happens when two different electronegative systems react. According to Table 4, the calculated value of ΔN is 0.879, indicating that the inhibitor molecules have a strong tendency to donate electrons to the metal's vacuum orbital [46].

The electron density surfaces generate the ESP, which is an important factor in defining the electrophilic and nucleophilic regions of the molecule [47]. Different colors determine the ESP of the ILB molecule, as shown in Figure 6. The red region represents the strongest repulsion, while the blue region represents the partially positive charge and the strongest attractions, the light blue region represents electron deficiency, the yellow region indicates that this part is slightly electron-rich, and the green region is neutral [48]. This demonstrates that ILB molecules have a strong affinity for metal surfaces and are resistant to electrophilic attack in general. This theoretical discovery supports and confirms the experimental findings.
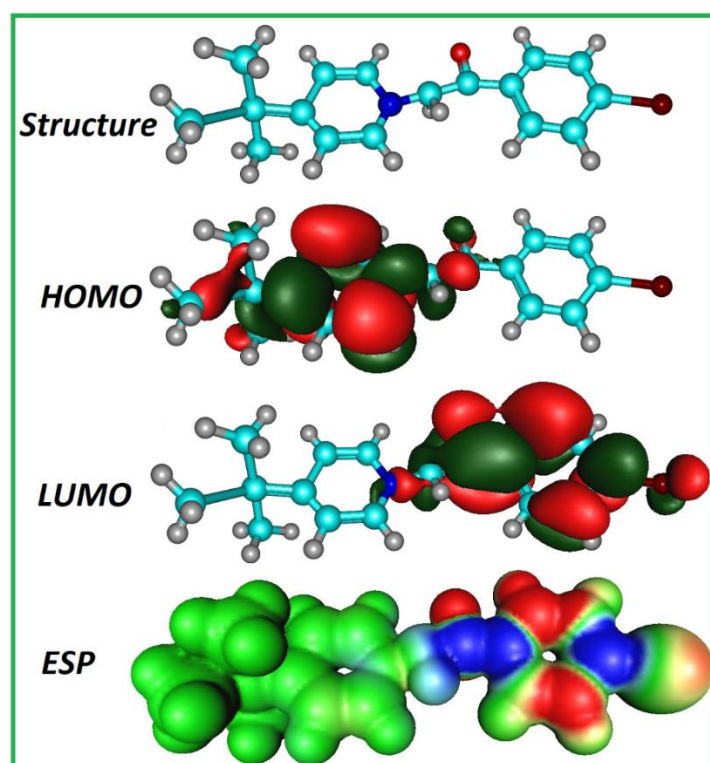
Figure 6. Equilibrium configurations, HOMO, LUMO, and ESP plots for ILB.

Table 4. Quantum chemical parameters calculated for ILB molecule.

Theoretical Parameters	ILB
E_{HOMO} (eV)	−5.606
E_{LUMO} (eV)	−1.930
ΔE (eV)	3.676
Ionization (I) (eV)	5.606
Affinity (A) (eV)	1.930
Absolute electronegativity (χ) (eV)	3.768
Global hardness (η) (eV)	1.838
Softness (σ)	0.544
ΔN	0.879

3.5.2. Molecular Dynamic Simulation (MDS)

MD simulations were performed to better understand the inhibitory process on the metal surface and to identify the low adsorption energy (E_{ads}) sites on the ions' surfaces. This enabled researchers to identify ILB's preferential adsorption. These techniques are frequently used to identify preferred adsorption sites on metal surfaces [49,50]. The simulation results, as well as the ILB molecule adsorption equilibrium configurations on the Fe surface, are shown in Figure 7. The inhibitor's adsorption orientation on the Fe surface was nearly flat, as shown in Figure 7. MD simulations reveal that the adsorption energy (E_{ads}) of ILB molecules is −13585.43 kcal mol^{-1}. ILB molecules demonstrate their high efficacy in preventing corrosion in steel by forming a strong chemical bond between the molecules and the Fe(110) surface. They also highlighted the effects of electronic transmission from the adsorbate to the substrate and dipole interactions [51,52].
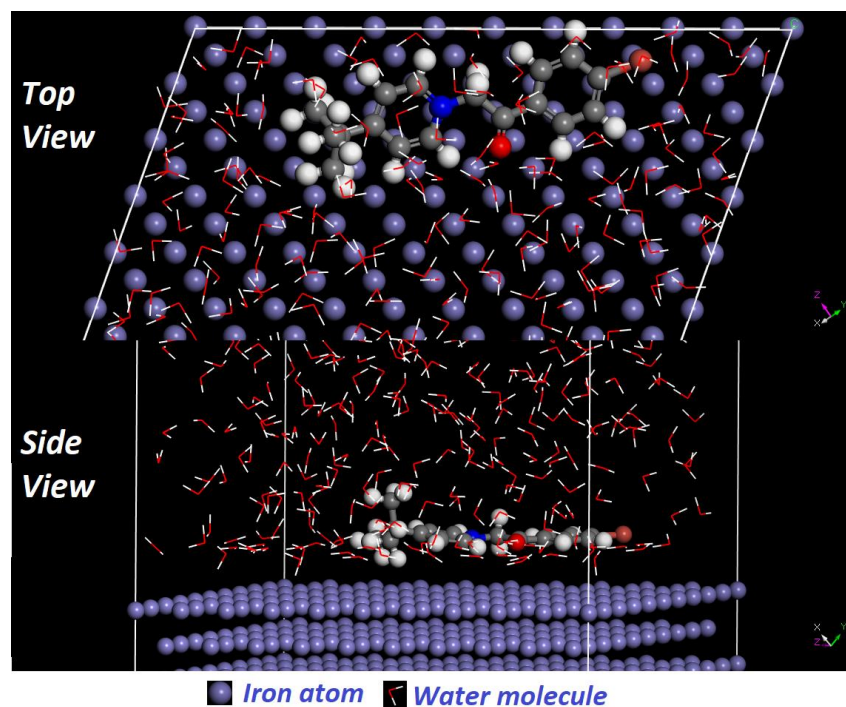
Figure 7. The optimized adsorption configuration of ILB molecule on Fe(1 1 0) plane.

3.6. Surface Characterization

3.6.1. Scanning Electron Microscopy (SEM) Measurements

The most well-known and commonly used surface analytical tool for surface characterization is the scanning electron microscope (SEM). Sharp surface pictures are often produced as a result of SEM analysis [53]. SEM micrographs of blank carbon steel surface inhibited with 1×10^{-3} M of ILB after 8 h of immersion are shown in Figure 8. The SEM image of the blank carbon steel surface (Figure 8a) revealed pits and cracks generated by an aggressive HCl attack on the metal, as well as extensively corroded and damaged areas. Despite this, SEM scans indicate that the inhibited carbon steel's surface (Figure 8b) is quite smooth. Because of the molecules' adsorption on the metal surface, the surfaces of steel specimens are smoother in the presence of ILB molecules [54].
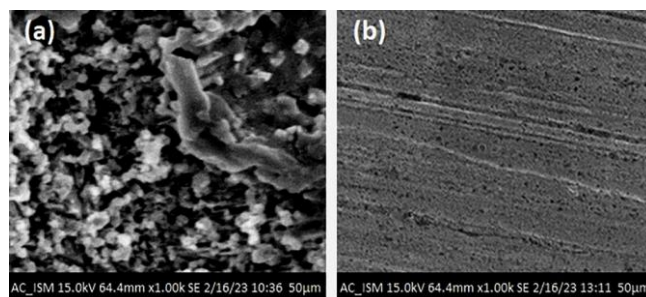

Figure 8. SEM images of carbon steel surfaces after 8 hours of immersion in: (**a**) aggressive HCl solution and, (**b**) aggressive HCl solution with 1×10^{-3} M of ILB 298 K.

3.6.2. Atomic Force Microscopy (AFM) Measurements

AFM is a powerful technique that is currently being utilised to investigate how inhibitors effect metal corrosion in a variety of electrolytic media [55]. Figure 9 depicts images taken with an atomic force microscope (AFM) of carbon steel surface before and after it was exposed to 1×10^{-3} M ILB for 8 h. When the metal surface was carefully examined, it was discovered to be completely corroded and destroyed (Figure 9a). This finding suggests that free aggressive HCl corrosion in the control solution had a substantial impact

on the metal surface. The surface roughness of the blank steel specimen was calculated to be 341 nm on average. However, in the AFM micrographs, the surface contour of the inhibited specimens seems quite smooth (Figure 9b). For the carbon steel samples inhibited with ILB molecules, the computed average surface roughness was 112 nm. The morphologies of the inhibited carbon steel specimens' surface significantly improved, proving that the inhibitor molecules under study create a shielding surface layer that protects the metal from the aggressive HCl solution and prevents corrosion [56].
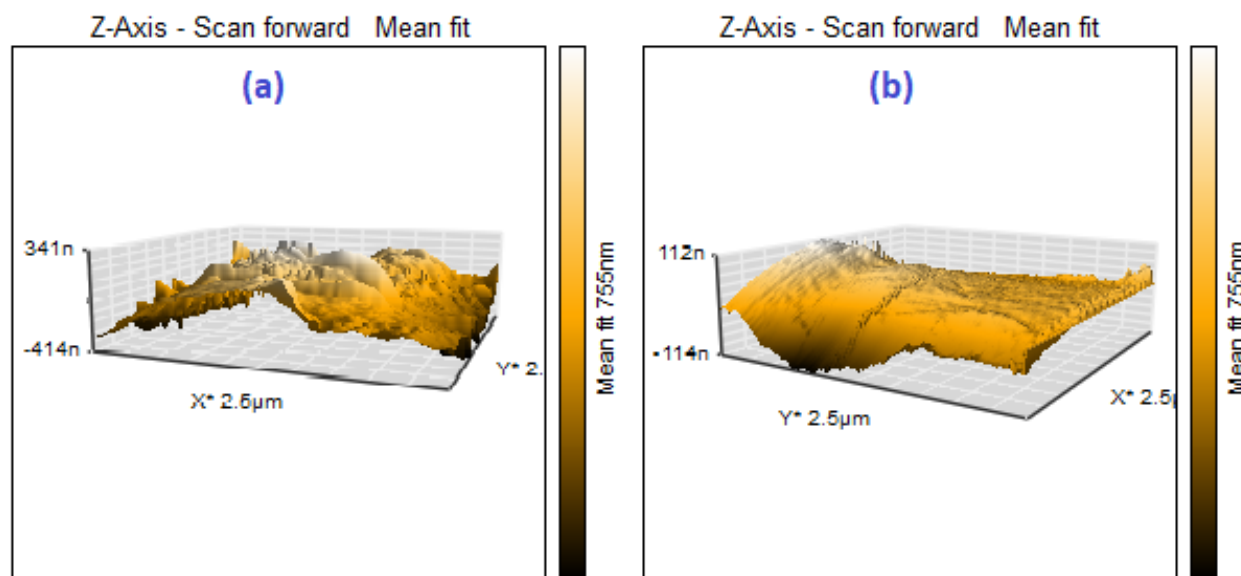

Figure 9. AFM images of carbon steel surfaces after 8 h of immersion in: (**a**) aggressive HCl solution, and (**b**) aggressive HCl solution with 1×10^{-3} M of ILB at 298 K.

3.7. Comparison with Previous Studies

The studied ILB corrosion inhibitor's efficacy for steel surface was compared to that of those previously reported. Table 5 details the inhibitor structure, corrosive solution, optimum inhibitor concentration, and inhibition efficacy as determined by several experimental methodologies [57–59]. ILB has a strong corrosion inhibition efficiency, which is visible even at low concentrations. This demonstrates that ILB has numerous potential uses in acid corrosion protection.

Table 5. Comparison the corrosion inhibition efficiency of studied ILB with other ILs obtained for steel in acidic media.

Inhibitors	Medium	Conc. (M)	η (%)	Ref
1-hexyl-3-methylimidazolium bis(trifluoromethyl-sulfonyl) imide	1 M HCl	3×10^{-4}	70.2	[57]
N-triethyl methylammonium acetate			70.4	[58]
1-Vinyl-3-butylimidazolium Bromide	1 M H$_2$SO$_4$		85.4	[59]
1-Vinyl-3-octadecylimidazolium Bromide			90.1	
1-Vinyl-3-docosylimidazolium Bromide			83.2	
1-Vinyl-3-dodecylimidazolium Bromide			94.4	
ILB	15% HCl		97.5	

4. Conclusions

Weight loss, electrochemical (EIS & PDP), and computational techniques were used to investigate the performance of the ionic liquid ILB as a potential corrosion inhibitor for carbon steel corrosion in aggressive HCl solution (15%) at 298 K. The inhibition efficiencies

evaluated from EIS, PDP, and WL tools were found to be: 97.9%, 97.3%, and 93.5%, respectively. ILB has good inhibitory performance as an acidizing corrosion inhibitor for carbon steel even at low dosing levels of 1×10^{-3} M. The ILB inhibitory action was set to be a mixed-type inhibitor. The Langmuir adsorption isotherm model is used to describe the adsorption of the ILB molecule. DFT can help ILB improve its inhibitory performance. The adsorption process was spontaneous. The results of both experimental and theoretical studies were agreed, which concluded that ILB is an effective green corrosion inhibitor for carbon steel in HCl media.

Author Contributions: Conceptualization, A.T., A.F. and A.A.F.; Data curation, A.T., A.F. and A.A.F.; Investigation, A.T., A.F., M.M.S.S. and A.A.F.; Methodology, A.T., A.F. and A.A.F.; Writing original draft, A.T., A.F. and A.A.F.; Writing- review editing, A.T., A.F., A.I.A., M.M.S.S., M.K. and A.A.F.; Formal analysis; A.T., A.F. and M.M.S.S.; Software; A.I.A. and M.K.; Funding acquisition, A.I.A.; Validation, A.T., A.F., A.A.F., A.I.A., M.K. and M.M.S.S. All authors have read and agreed to the published version of the manuscript.

Data Availability Statement: Not applicable.

Conflicts of Interest: The authors declare no conflict of interest.

References

1. Costa, E.M.; Dedavid, B.A.; Santos, C.A.; Lopes, N.F.; Fraccaro, C.; Pagartanidis, T.; Lovatto, L.P. Crevice corrosion on stainless steels in oil and gas industry: A review of techniques for evaluation, critical environmental factors and dissolved oxygen. *Eng. Fail. Anal.* **2023**, *144*, 106955. https://doi.org/10.1016/j.engfailanal.2022.106955.

2. Farag, A.A.; Eid, A.; Shaban, M.; Mohamed, E.A.; Raju, G. Integrated modeling, surface, electrochemical, and biocidal investigations of novel benzothiazoles as corrosion inhibitors for shale formation well stimulation. *J. Mol. Liq.* **2021**, *336*, 116315. https://doi.org/10.1016/j.molliq.2021.116315.

3. Toghan, A.; Gouda, M.; Shalabi, K.; El-Lateef, H.M.A. Preparation, Characterization, and Evaluation of Macrocrystalline and Nanocrystalline Cellulose as Potential Corrosion Inhibitors for SS316 Alloy during Acid Pickling Process: Experimental and Computational Methods. *Polymers* **2021**, *13*, 2275. https://doi.org/10.3390/polym13142275.

4. El-Lateef, H.M.A.; El-Beltagi, H.S.; Mohamed, M.E.M.; Kandeel, M.; Bakir, E.; Toghan, A.; Shalabi, K.; Tantawy, A.H.; Khalaf, M.M. Novel Natural Surfactant-Based Fatty Acids and Their Corrosion-Inhibitive Characteristics for Carbon Steel-Induced Sweet Corrosion: Detailed Practical and Computational Explorations. *Front. Mater.* **2022**, *9*, 29. https://doi.org/10.3389/fmats.2022.843438.

5. Saleh, T.A.; Haruna, K.; Alharbi, B. Diaminoalkanes functionalized graphene oxide as corrosion inhibitors against carbon steel corrosion in simulated oil/gas well acidizing environment. *J. Colloid Interface Sci.* **2023**, *630*, 591–610. https://doi.org/10.1016/j.jcis.2022.10.054.

6. Odewunmi, N.A.; Mazumder, M.A.; Ali, S.A. Tipping effect of tetra-alkylammonium on the potency of N-(6-(1H-benzo[d]imidazol-1-yl)hexyl)-N, N-dimethyldodecan-1-aminium bromide (BIDAB) as corrosion inhibitor of austenitic 304L stainless steel in oil and gas acidization: Experimental and DFT approach. *J. Mol. Liq.* **2022**, *360*, 119431. https://doi.org/10.1016/j.molliq.2022.119431.

7. Al-Sabagh, A.M.; Abdou, M.I.; Migahed, M.A.; Fadl, A.M.; Farag, A.A.; Mohammedy, M.M.; Abd-Elwanees, S.; Deiab, A. Influence of ilmenite ore particles as pigment on the anticorrosion and mechanical performance properties of polyamine cured epoxy for internal coating of gas transmission pipelines. *Egypt. J. Pet.* **2018**, *27*, 415–425. https://doi.org/10.1016/j.ejpe.2017.07.005.

8. El-Lateef, H.M.A.; Shaaban, S.; Khalaf, M.M.; Toghan, A.; Shalabi, K. Synthesis, experimental, and computational studies of water soluble anthranilic organoselenium compounds as safe corrosion inhibitors for J55 pipeline steel in acidic oilfield formation water. *Colloids Surf. A Physicochem. Eng. Asp.* **2021**, *625*, 126894. https://doi.org/10.1016/j.colsurfa.2021.126894.

9. Zhang, Q.H.; Li, Y.Y.; Lei, Y.; Wang, X.; Liu, H.F.; Zhang, G.A. Comparison of the synergistic inhibition mechanism of two eco-friendly amino acids combined corrosion inhibitors for carbon steel pipelines in oil and gas production. *Appl. Surf. Sci.* **2022**, *583*, 152559. https://doi.org/10.1016/j.apsusc.2022.152559.

10. Heikal, M.; Ali, A.; Ibrahim, B.; Toghan, A. Electrochemical and physico-mechanical characterizations of fly ash-composite cement. *Constr. Build. Mater.* **2020**, *243*, 118309.

11. Silva, R.M.P.; Suffredini, H.B.; Bastos, I.N.; Santos, L.F.; Simões, A.M.P. Naphthenic acid corrosion of API 5L X70 steel in aqueous/oil environment using electrochemical surface-resolved and analytical techniques. *Electrochim. Acta* **2022**, *407*, 139900. https://doi.org/10.1016/j.electacta.2022.139900.

12. Farag, A. Oil-in-water emulsion of a heterocyclic adduct as a novel inhibitor of API X52 steel corrosion in acidic solution. *Corros. Rev.* **2018**, *36*, 575–588. https://doi.org/10.1515/corrrev-2018-0002.

13. Altalhi, A.A.; Mohammed, E.A.; Morsy, S.S.M.; Negm, N.A.; Farag, A.A. Catalyzed production of different grade biofuels using metal ions modified activated carbon of cellulosic wastes. *Fuel* **2021**, *295*, 120646. https://doi.org/10.1016/j.fuel.2021.120646.

14. Toghan, A.; Gadow, H.S.; Dardeer, H.M.; Elabbasy, H.M. New promising halogenated cyclic imides derivatives as potential corrosion inhibitors for carbon steel in hydrochloric acid solution. *J. Mol. Liq.* **2021**, *325*, 115136. https://doi.org/10.1016/j.molliq.2020.115136.

15. Li, E.; Li, Y.; Liu, S.; Yao, P. Choline amino acid ionic liquids as green corrosion inhibitors of mild steel in acidic medium. *Colloids Surfaces A: Physicochem. Eng. Asp.* **2023**, *657*, 130541. https://doi.org/10.1016/j.colsurfa.2022.130541.

16. Toghan, A.; Fawzy, A.; Al Bahir, A.; Alqarni, N.; Sanad, M.M.S.; Khairy, M.; Alakhras, A.I.; Farag, A.A. Computational Foretelling and Experimental Implementation of the Performance of Polyacrylic Acid and Polyacrylamide Polymers as Eco-Friendly Corrosion Inhibitors for Copper in Nitric Acid. *Polymers* **2022**, *14*, 4802. https://doi.org/10.3390/polym14224802.

17. Fawzy, A.; Toghan, A.; Alqarni, N.; Morad, M.; Zaki, M.E.A.; Sanad, M.M.S.; Alakhras, A.I.; Farag, A.A. Experimental and Computational Exploration of Chitin, Pectin, and Amylopectin Polymers as Efficient Eco-Friendly Corrosion Inhibitors for Mild Steel in an Acidic Environment: Kinetic, Thermodynamic, and Mechanistic Aspects. *Polymers* **2023**, *15*, 891. https://doi.org/10.3390/polym15040891.

18. Al-Gamal, A.G.; Farag, A.A.; Elnaggar, E.M.; Kabel, K.I. Comparative impact of doping nano-conducting polymer with carbon and carbon oxide composites in alkyd binder as anti-corrosive coatings. *Compos. Interfaces* **2018**, *25*, 959–980. https://doi.org/10.1080/09276440.2018.1450578.

19. Farag, A.A.; Mohamed, E.A.; Toghan, A. The new trends in corrosion control using superhydrophobic surfaces: A review. *Corros. Rev.* **2022**, *41*, 21–37. https://doi.org/10.1515/corrrev-2022-0020.

20. Amer, A.; Sayed, G.H.; Ramadan, R.M.; Rabie, A.M.; Negm, N.A.; Farag, A.A.; Mohammed, E.A. Assessment of 3-amino-1H-1,2,4-triazole modified layered double hydroxide in effective remediation of heavy metal ions from aqueous environment. *J. Mol. Liq.* **2021**, *341*, 116935. https://doi.org/10.1016/j.molliq.2021.116935.

21. Farag, A.A.; Afif, A.G.; Salih, S.A.; Altalhi, A.A.; Mohamed, E.A.; Mohamed, G.G. Highly Efficient Elimination of Pb^{+2} and Al^{+3} Metal Ions from Wastewater Using Graphene Oxide/3,5-Diaminobenzoic Acid Composites: Selective Removal of Pb^{2+} from Real Industrial Wastewater. *ACS Omega* **2022**, *7*, 38347–38360. https://doi.org/10.1021/acsomega.2c03150.

22. Wahab, M.M.A.; Sayed, G.H.; Ramadan, R.M.; Mady, A.H.; Rabie, A.M.; Farag, A.A.; Negm, N.A.; Mohamed, E.A. Synergistic effects of graphene oxide grafted with barbituric acid nanocomposite for removal of heavy metals from aqueous solution. *Nanotechnol. Environ. Eng.* **2022**, 1–13.

23. Haldhar, R.; Raorane, C.J.; Mishra, V.; Periyasamy, T.; Berisha, A.; Kim, S.-C. Development of different chain lengths ionic liquids as green corrosion inhibitors for oil and gas industries: Experimental and theoretical investigations. *J. Mol. Liq.* **2023**, *372*, 121168. https://doi.org/10.1016/j.molliq.2022.121168.

24. Berdimurodov, E.; Kholikov, A.; Akbarov, K.; Guo, L.; Kaya, S.; Katin, K.P.; Verma, D.K.; Rbaa, M.; Dagdag, O.; Haldhar, R. Novel bromide–cucurbit[7]uril supramolecular ionic liquid as a green corrosion inhibitor for the oil and gas industry. *J. Electroanal. Chem.* **2021**, *901*, 115794. https://doi.org/10.1016/j.jelechem.2021.115794.

25. Farag, A.A.; Badr, E.A. Non-ionic surfactant loaded on gel capsules to protect downhole tubes from produced water in acidizing oil wells. *Corros. Rev.* **2020**, *38*, 151–164. https://doi.org/10.1515/corrrev-2019-0030.

26. Mohamed, H.A.; Farag, A.A.; Badran, B.M. Corrosion inhibition of mild steel using emulsified thiazole adduct in Different binder systems. *Eurasian Chem.* **2008**, *10*, 67–77.

27. ASTM International. Standard Practice for Preparing, Cleaning, and Evaluating Corrosion Test. *Significance* **1999**, *90*, 1–9. https://doi.org/10.1520/G0001-03R11.2.

28. Toghan, A.; Khairy, M.; Huang, M.; Gadow, H. Electrochemical, surface analysis, and theoretical investigation of 3-hydroxy-5-(phenylamino)-4-(p-tolyldiazenyl)thiophen-2-yl)(phenyl)methanone as a corrosion inhibitor for carbon steel in a molar hydrochloric acid solution. *Int. J. Electrochem. Sci.* **2023**, *18*, 100070. https://doi.org/10.1016/j.ijoes.2023.100070.

29. Aslam, R.; Mobin, M.; Huda; Shoeb, M.; Murmu, M.; Banerjee, P. Proline nitrate ionic liquid as high temperature acid corrosion inhibitor for mild steel: Experimental and molecular-level insights. *J. Ind. Eng. Chem.* **2021**, *100*, 333–350. https://doi.org/10.1016/j.jiec.2021.05.005.

30. Toghan, A. Inhibition Effects of Citrulline and Glutamine for Mild Steel Corrosion in Sulfuric Acid Environment: Thermodynamic and Kinetic Aspects. *Int. J. Electrochem. Sci.* **2021**, *16*, 211118. https://doi.org/10.20964/2021.11.40.

31. Kannan, P.; Varghese, A.; Palanisamy, K.; Abousalem, A.S. Probing the effect of newly synthesized phenyltrimethylammonium tetrachloroaluminate ionic liquid as an inhibitor for carbon steel corrosion. *Appl. Surf. Sci. Adv.* **2021**, *6*, 100150. https://doi.org/10.1016/j.apsadv.2021.100150.

32. Mohamed, E.A.; Hashem, H.E.; Azmy, E.M.; Negm, N.A.; Farag, A.A. Synthesis, structural analysis, and inhibition approach of novel eco-friendly chalcone derivatives on API X65 steel corrosion in acidic media assessment with DFT & MD studies. *Environ. Technol. Innov.* **2021**, *24*, 101966. https://doi.org/10.1016/j.eti.2021.101966.

33. Toghan, A.; Khairy, M.; Huang, M.; Farag, A.A. Electrochemical, chemical and theoretical exploration of the corrosion inhibition of carbon steel with new imidazole-carboxamide derivatives in an acidic environment. *Int. J. Electrochem. Sci.* **2023**, *18*, 100072 https://doi.org/10.1016/j.ijoes.2023.100072.

34. Fawzy, A.; Toghan, A. Inhibition Evaluation of Chromotrope Dyes for the Corrosion of Mild Steel in an Acidic Environment: Thermodynamic and Kinetic Aspects. *ACS Omega* **2021**, *6*, 4051–4061. https://doi.org/10.1021/acsomega.0c06121.

35. Mobin, M.; Aslam, R.; Salim, R.; Kaya, S. An investigation on the synthesis, characterization and anti-corrosion properties of choline based ionic liquids as novel and environmentally friendly inhibitors for mild steel corrosion in 5% HCl. *J. Colloid Interface Sci.* **2022**, *620*, 293–312. https://doi.org/10.1016/j.jcis.2022.04.036.

36. Riggs, O.L., Jr; Nathan, C.C. *Corrosion Inhibitors*; CC Nathan: Houston, TX, USA, 1973.

37. Souza, L.; Pereira, E.; Matlakhova, L.; Nicolin, V.A.; Monteiro, S.N.; de Azevedo, A.R. Ionic liquids as corrosion inhibitors for carbon steel protection in hydrochloric acid solution: A first review. *J. Mater. Res. Technol.* **2023**, *22*, 2186–2205. https://doi.org/10.1016/j.jmrt.2022.12.066.

38. Koundal, M.; Singh, A.; Sharma, C. Study on the effect of imidazolium ionic liquid as a modulator of corrosion inhibition of anionic surfactant sodium dodecyl sulfate (SDS) on mild steel in sodium chloride solution. *J. Mol. Liq.* **2022**, *350*, 118561. https://doi.org/10.1016/j.molliq.2022.118561.

39. Mazumder, M.A.J. Synthesis, characterization and electrochemical analysis of cysteine modified polymers for corrosion inhibition of mild steel in aqueous 1 M HCl. *RSC Adv.* **2019**, *9*, 4277–4294. https://doi.org/10.1039/C8RA09833F.

40. Singh, A.K.; Chugh, B.; Thakur, S.; Pani, B.; Lgaz, H.; Chung, I.-M.; Pal, S.; Prakash, R. Green approach of synthesis of thiazolyl imines and their impeding behavior against corrosion of mild steel in acid medium. *Colloids Surf. A Physicochem. Eng. Asp.* **2020**, *599*, 124824. https://doi.org/10.1016/j.colsurfa.2020.124824.

41. Verma, C.; Ebenso, E.E.; Quraishi, M. Molecular structural aspects of organic corrosion inhibitors: Influence of –CN and –NO2 substituents on designing of potential corrosion inhibitors for aqueous media. *J. Mol. Liq.* **2020**, *316*, 113874. https://doi.org/10.1016/j.molliq.2020.113874.

42. Shaban, M.M.; Negm, N.A.; Farag, R.K.; Fadda, A.A.; Gomaa, A.E.; Farag, A.A.; Migahed, M.A. Anti-corrosion, antiscalant and anti-microbial performance of some synthesized trimeric cationic imidazolium salts in oilfield applications. *J. Mol. Liq.* **2022**, *351*, 118610. https://doi.org/10.1016/j.molliq.2022.118610.

43. Farag, A.A.; Ismail, A.S.; Migahed, M.A. Squid By-product Gelatin Polymer as an Eco-friendly Corrosion Inhibitor for Carbon Steel in 0.5 M H2SO4 Solution: Experimental, Theoretical, and Monte Carlo Simulation Studies. *J. Bio- Tribo-Corrosion* **2019**, *6*, 1–15. https://doi.org/10.1007/s40735-019-0310-0.

44. Farag, A.A.; Abdallah, H.E.; Badr, E.A.; Mohamed, E.A.; Ali, A.I.; El-Etre, A. The inhibition performance of morpholinium derivatives on corrosion behavior of carbon steel in the acidized formation water: Theoretical, experimental and biocidal evaluations. *J. Mol. Liq.* **2021**, *341*, 117348. https://doi.org/10.1016/j.molliq.2021.117348.

45. Hsissou, R.; Benhiba, F.; Dagdag, O.; El Bouchti, M.; Nouneh, K.; Assouag, M.; Briche, S.; Zarrouk, A.; Elharfi, A. Development and potential performance of prepolymer in corrosion inhibition for carbon steel in 1.0 M HCl: Outlooks from experimental and computational investigations. *J. Colloid Interface Sci.* **2020**, *574*, 43–60. https://doi.org/10.1016/j.jcis.2020.04.022.

46. Hashem, H.E.; Farag, A.A.; Mohamed, E.A.; Azmy, E.M. Experimental and theoretical assessment of benzopyran compounds as inhibitors to steel corrosion in aggressive acid solution. *J. Mol. Struct.* **2021**, *1249*, 131641. https://doi.org/10.1016/j.molstruc.2021.131641.

47. Hsissou, R.; Azogagh, M.; Benhiba, F.; Echihi, S.; Galai, M.; Shaim, A.; Bahaj, H.; Briche, S.; Kaya, S.; Serdaroğlu, G.; et al. Insight of development of two cured epoxy polymer composite coatings as highly protective efficiency for carbon steel in sodium chloride solution: DFT, RDF, FFV and MD approaches. *J. Mol. Liq.* **2022**, *360*, 119406. https://doi.org/10.1016/j.molliq.2022.119406.

48. Nadi, I.; Bouanis, M.; Benhiba, F.; Nohair, K.; Nyassi, A.; Zarrouk, A.; Jama, C.; Bentiss, F. Insights into the inhibition mechanism of 2,5-bis(4-pyridyl)-1,3,4-oxadiazole for carbon steel corrosion in hydrochloric acid pickling via experimental and computational approaches. *J. Mol. Liq.* **2021**, *342*, 116958. https://doi.org/10.1016/j.molliq.2021.116958.

49. Toghan, A.; Fawzy, A.; Alakhras, A.I.; Farag, A.A. Electrochemical and Theoretical Examination of Some Imine Compounds as Corrosion Inhibitors for Carbon Steel in Oil Wells Formation Water. *Int. J. Electrochem. Sci.* **2022**, *17*, 2212108. https://doi.org/10.20964/2022.12.94.

50. EL Hajjaji, F.; Ech-Chihbi, E.; Salim, R.; Titi, A.; Messali, M.; El Ibrahimi, B.; Kaya, S.; Taleb, M. A detailed electronic-scale DFT modeling/MD simulation, electrochemical and surface morphological explorations of imidazolium-based ionic liquids as sustainable and non-toxic corrosion inhibitors for mild steel in 1 M HCl. *Mater. Sci. Eng. B* **2023**, *289*, 116232. https://doi.org/10.1016/j.mseb.2022.116232.

51. Farag, A.A.; Toghan, A.; Mostafa, M.S.; Lan, C.; Ge, G. Environmental Remediation through Catalytic Inhibition of Steel Corrosion by Schiff's Bases: Electrochemical and Biological Aspects. *Catalysts* **2022**, *12*, 838. https://doi.org/10.3390/catal12080838.

52. Lakbaibi, Z.; Damej, M.; Molhi, A.; Benmessaoud, M.; Tighadouini, S.; Jaafar, A.; Benabbouha, T.; Ansari, A.; Driouich, A.; Tabyaoui, M. Evaluation of inhibitive corrosion potential of symmetrical hydrazine derivatives containing nitrophenyl moiety in 1M HCl for C38 steel: Experimental and theoretical studies. *Heliyon* **2022**, *8*, e09087. https://doi.org/10.1016/j.heliyon.2022.e09087.

53. Mobin, M.; Rizvi, M. Polysaccharide from Plantago as a green corrosion inhibitor for carbon steel in 1M HCl solution. *Carbohydr. Polym.* **2017**, *160*, 172–183. https://doi.org/10.1016/j.carbpol.2016.12.056.

54. Zarei, A.; Dehghani, A.; Guo, L.; Ramezanzadeh, B. Pepper extract effectiveness as a natural inhibitor against corrosion of steel samples (SS) in 1 M hydrochloric acid; Theoretical (DFT calculation—MD simulation), thermodynamic, and electrochemical-surface studies. *Ind. Crop. Prod.* **2022**, *189*, 115839. https://doi.org/10.1016/j.indcrop.2022.115839.

55. Singh, A.K.; Quraishi, M. Investigation of the effect of disulfiram on corrosion of mild steel in hydrochloric acid solution. *Corros. Sci.* **2011**, *53*, 1288–1297. https://doi.org/10.1016/j.corsci.2011.01.002.

56. Ouakki, M.; Galai, M.; Benzekri, Z.; Arribou, Z.; Ech-Chihbi, E.; Guo, L.; Dahmani, K.; Nouneh, K.; Briche, S.; Boukhris, S.; et al. A detailed investigation on the corrosion inhibition effect of by newly synthesized pyran derivative on mild steel in 1.0 M HCl: Experimental, surface morphological (SEM-EDS, DRX& AFM) and computational analysis (DFT & MD simulation). *J. Mol. Liq.* **2021**, *344*, 117777. https://doi.org/10.1016/j.molliq.2021.117777.

57. Murulana, L.C.; Singh, A.K.; Shukla, S.K.; Kabanda, M.; Ebenso, E.E. Experimental and Quantum Chemical Studies of Some Bis(trifluoromethyl-sulfonyl) Imide Imidazolium-Based Ionic Liquids as Corrosion Inhibitors for Mild Steel in Hydrochloric Acid Solution. *Ind. Eng. Chem. Res.* **2012**, *51*, 13282–13299. https://doi.org/10.1021/ie300977d.

58. Olivares-Xometl, O.; López-Aguilar, C.; Herrastí-González, P.; Likhanova, N.V.; Lijanova, I.; Martínez-Palou, R.; Rivera-Márquez, J.A. Adsorption and corrosion inhibition performance by three new ionic liquids on API 5L X52 steel surface in acid media. *Ind. Eng. Chem. Res.* **2014**, *53*, 9534–9543.

59. Guzmán-Lucero, D.; Olivares-Xometl, O.; Martínez-Palou, R.; Likhanova, N.V.; Domínguez-Aguilar, M.A.; Garibay-Febles, V. Synthesis of selected vinylimidazolium ionic liquids and their effectiveness as corrosion inhibitors for carbon steel in aqueous sulfuric acid. *Ind. Eng. Chem. Res.* **2011**, *50*, 7129–7140.